Minimizing Actuator-Induced Residual Error in Active Space Telescope Primary Mirrors

Aero/Astro Research Evaluation

Matthew W. Smith
m_smith@mit.edu

Advisor:
Prof. David W. Miller

Outline

- **Background:** Large telescopes
- **Motivation and Research Question:** Lightweight error-free mirrors
- **Literature Review**
- **Approach:** Parametric FE modeling
- **Results:** Rib shaping
- **Conclusion**

Background

- Trend toward large aperture space telescopes
  - Higher resolving power
  - Increased light-gathering ability
  - Launch constraints drive new technology for segmented mirrors and *low areal density*

Previous generation:
Hubble Space Telescope (HST)


[1]


[1]

Material: Ultra low expansion (ULE) glass
Areal density: 180 kg/m^2
Diameter: 2.4 m
Shape control: passive
Actuators: none

Current generation:
James Webb Space Telescope (JWST)

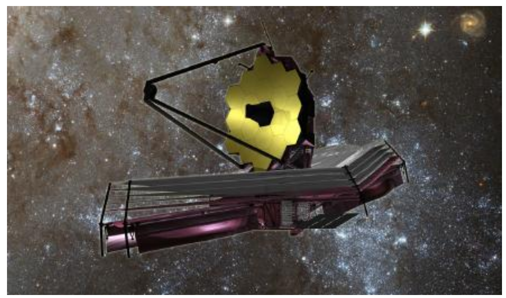
[1]

[2]

Material: Beryllium
Areal density: ~30 kg/m^2
Diameter: 6.5 m (1.3 m segments)
Shape control: active (7 DOF)
Actuators: cryogenic stepper motors

Next generation:
"Highly Integrated" Mirror Design

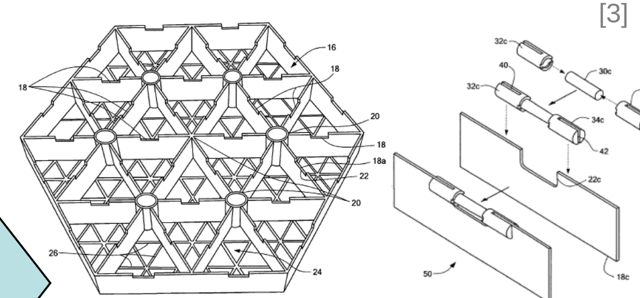
[3]

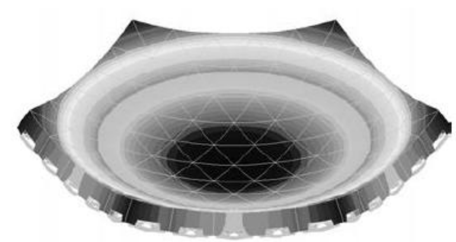
[4]

Material: Silicon Carbide (SiC)
Areal density: <15 kg/m^2
Diameter: 1 m segments (baseline)
Shape control: active (100+ DOF)
Actuators: piezoelectric stacks

Motivation and Research Objective

- Low areal density requires active shape control
  - Correct quasi-static disturbances (thermal)
  - Correct manufacturing errors (SiC casting process)
- Problem: actuator-induced residual error
  - Symptom of discrete actuators commanding low-order shapes
  - Degrades image sharpness

Actuator-induced residual error (actual – desired)

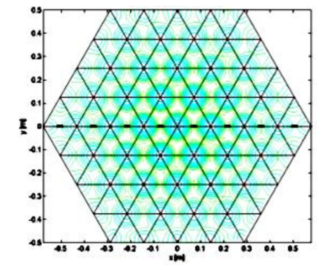

Un-actuated mirror

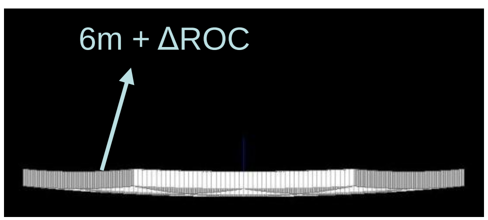

Desired surface change

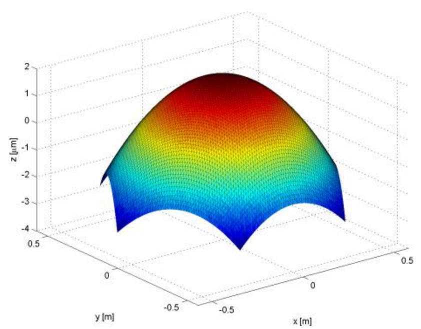

Actual surface change

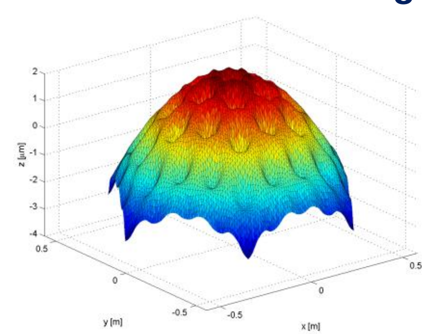

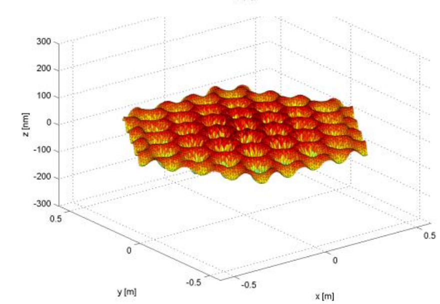

Research Objective
To reduce actuator-induced high spatial frequency residual error
by taking advantage of changes in mirror geometry
using a parametric finite element mirror model
while keeping areal density (mass) and number of actuators (power, complexity) constant.

Relationship with Prior Work

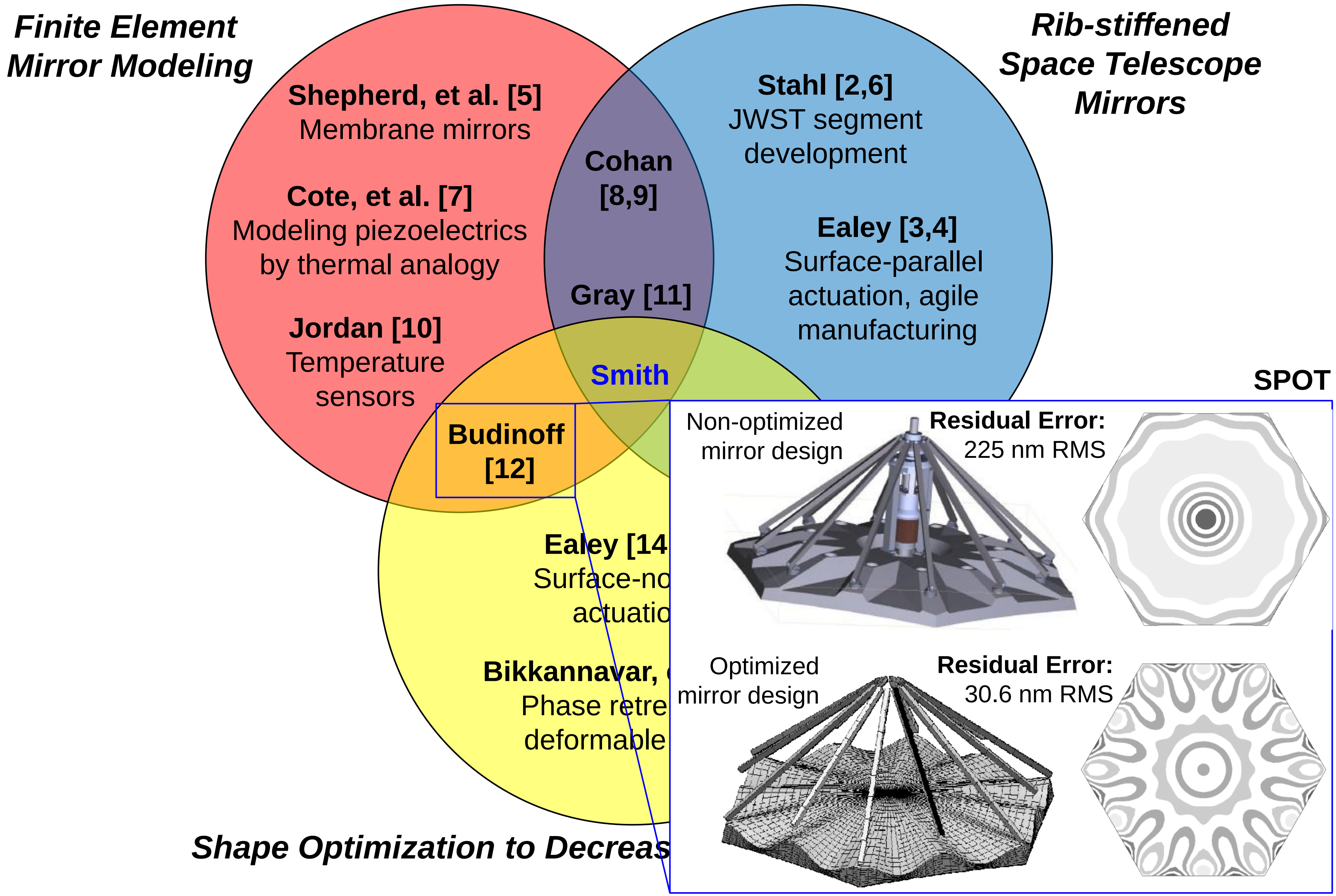

Approach

Research Objective
To reduce actuator-induced high spatial frequency residual error
by taking advantage of changes in mirror geometry
using a parametric finite element mirror model
while keeping areal density (mass) and number of actuators (power, complexity) constant.

- Model of primary mirror
  - Parameterization allows for rapid iteration

Parameter file

- Areal density [kg/m^2]
- Number of actuators
- Rib shaping function
- Diameter [m]
- …

Finite Element Mirror Model

Figure of merit

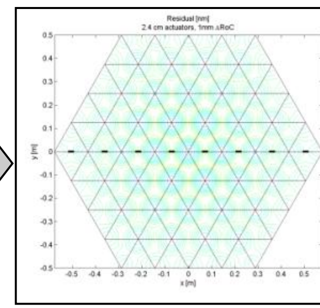

Residual error [nm RMS]

Final design

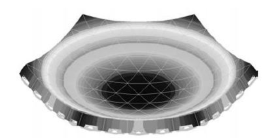

Iterate

Vary parameters of interest

Approach (cont.)

- Mirror model details
  - Varying the rib shaping function

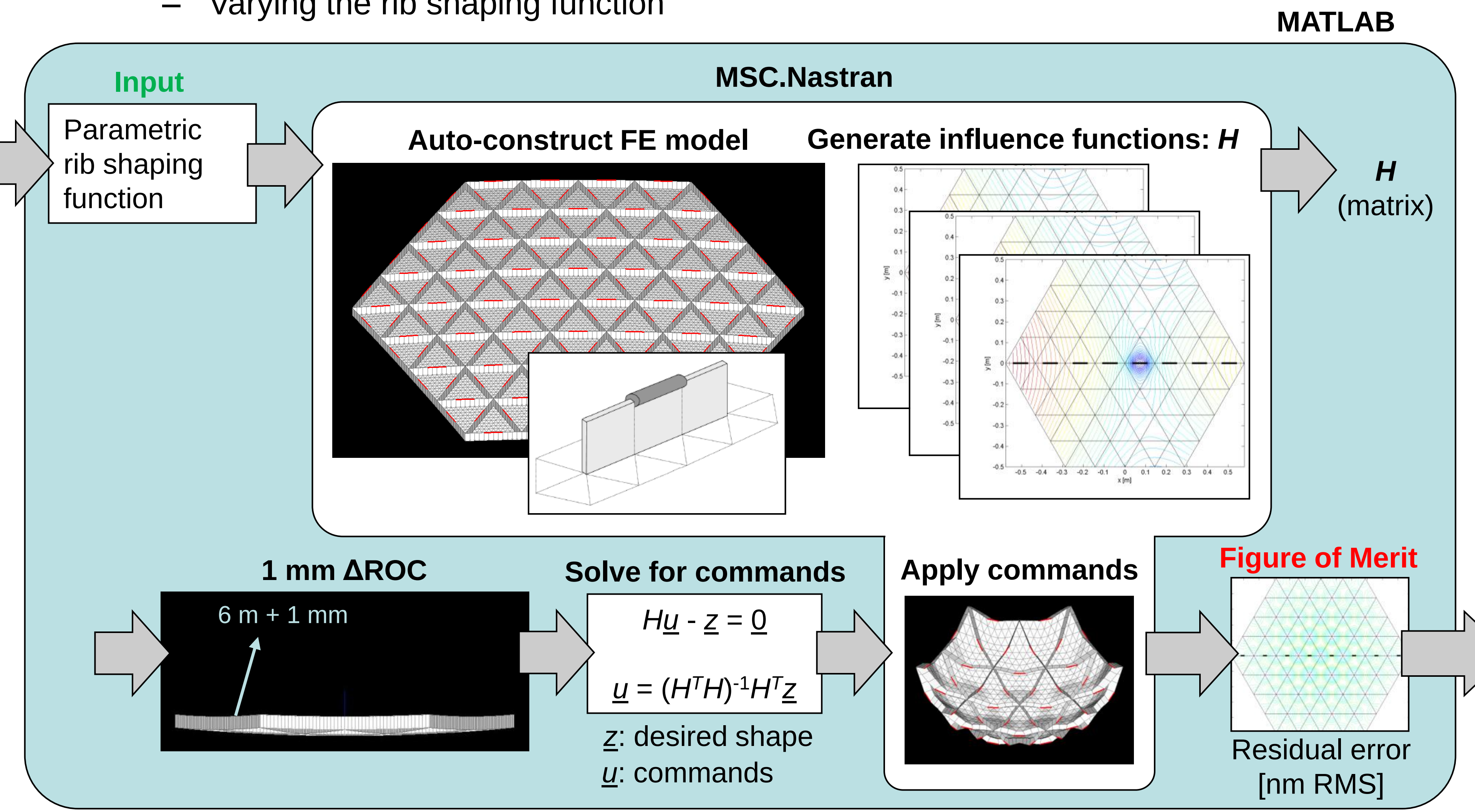

Setup

- Sinusoidal rib shaping
  - Idea: spread the load/influence of a localized actuator further along a rib
  - Parameterize shaping function by amplitude *a* (0 mm ≤ *a* ≤ 20 mm)
  - Areal density stays constant

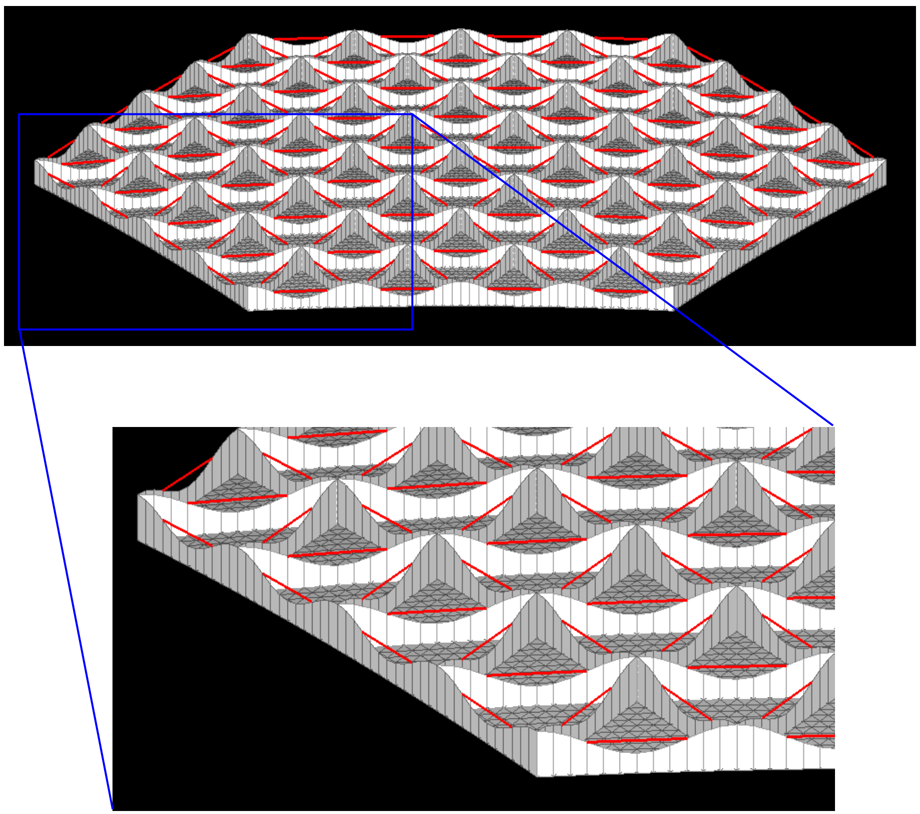

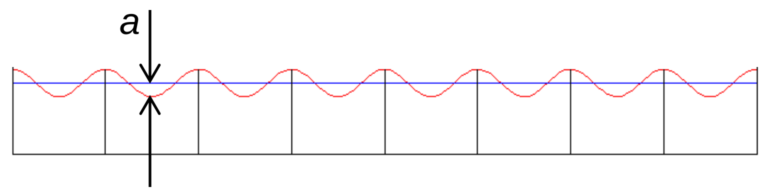

Results

- Sinusoidal shaping function
  - *a* = 12.5 mm minimizes residual error (27% reduction compared to the baseline)

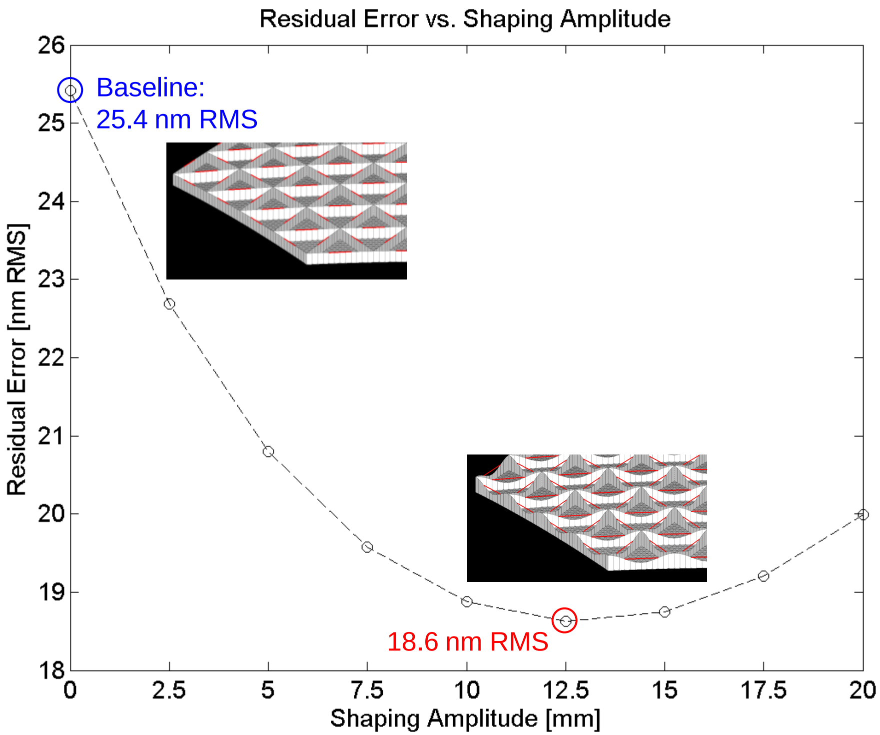

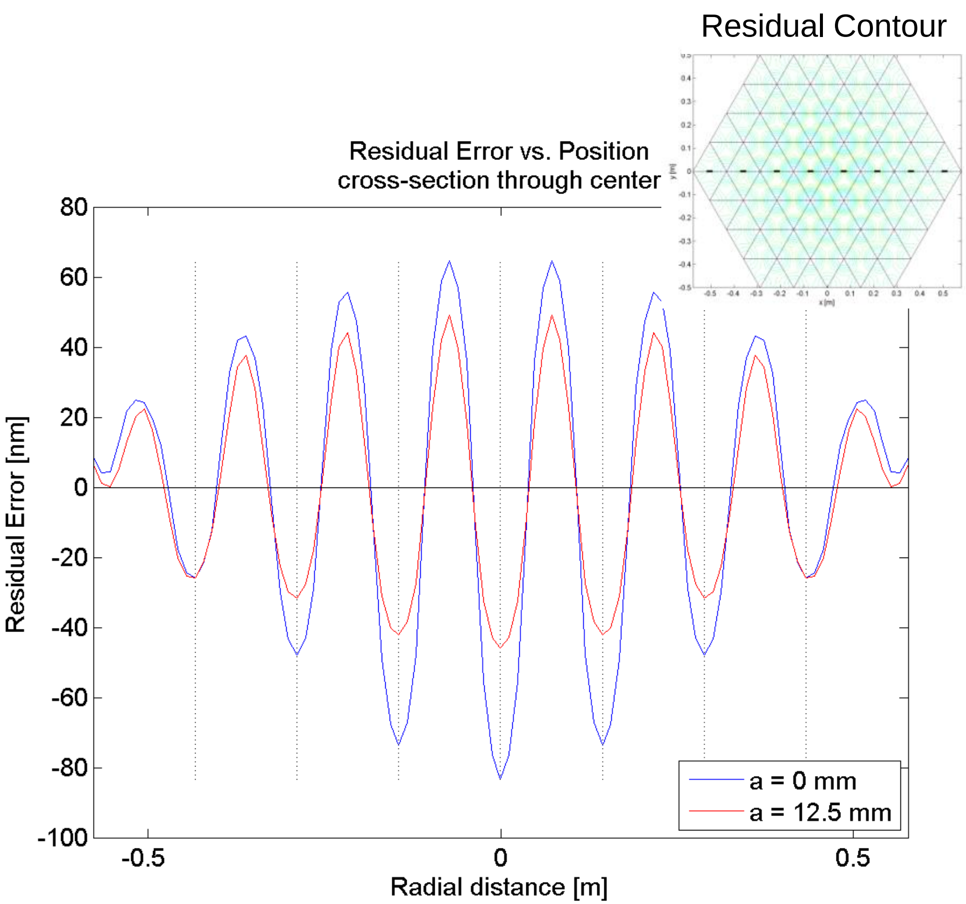

Results (cont.)

- Sinusoidal shaping function
  - Reason for improvement: “broader” influence function
  - Actuator becomes less “discrete”

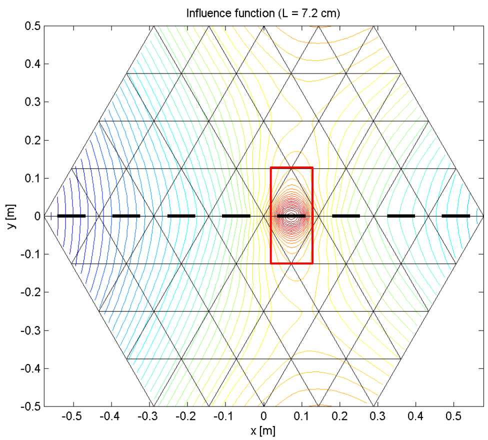

Influence Function

a = 0 mm

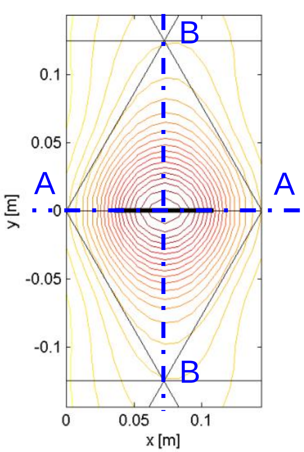

a = 12.5 mm

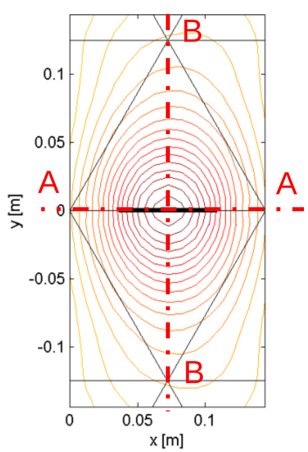

Slice A-A (horizontal)

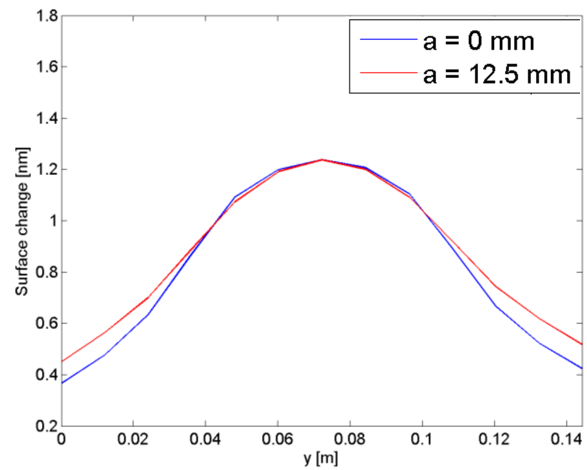

Slice B-B (vertical)

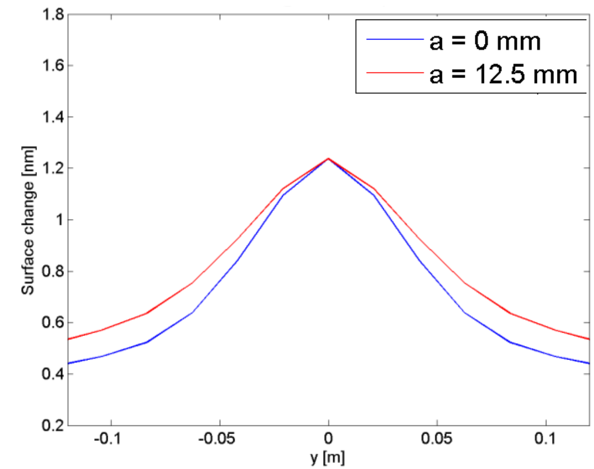

Conclusion

Research Objective
To reduce actuator-induced high spatial frequency residual error
by taking advantage of changes in mirror geometry
using a parametric finite element mirror model
while keeping areal density (mass) and number of actuators (power, complexity) constant.

- Sinusoidal rib shaping
  - Rib shaping can reduce residual error
  - Mass is constant
  - Number of actuators is constant
  - a = 12.5 mm (best case) reduces residual by 27%
  - Broadens influence functions and “spreads” the effect of discrete actuators

Conclusion (cont.)

Research Objective
To reduce actuator-induced high spatial frequency residual error
by taking advantage of changes in mirror geometry
using a parametric finite element mirror model
while keeping areal density (mass) and number of actuators (power, complexity) constant.

- Path ahead
  - Rib shaping: Explore additional “basis functions” for ribs and optimize for best combination (e.g. series of cosines)

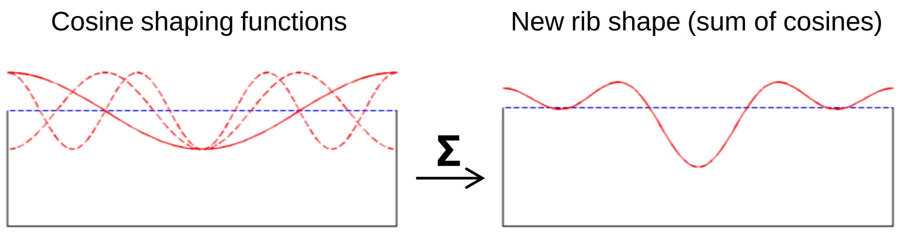

  - Rib blending: Blend the ribs smoothly into the facesheet, instead of the current 90° junction

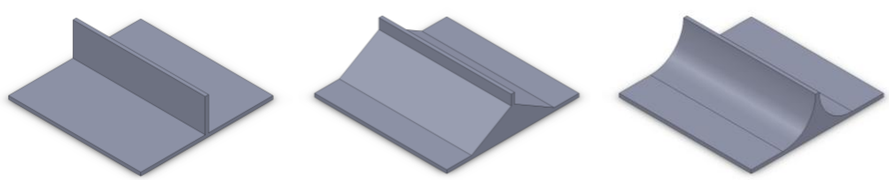

  - General shape optimization: Using parameterized rib shaping and blending functions, optimize to find mirror shape that best reduces actuator-induced residual, while meeting stiffness requirements

Conclusion (cont.)

Research Objective
To reduce actuator-induced high spatial frequency residual error
by taking advantage of changes in mirror geometry
using a parametric finite element mirror model
while keeping areal density (mass) and number of actuators (power, complexity) constant.

- Expected contributions
  - Set of optimized mirror shapes that reduce actuator-induced residual error (constant mass and constant number of actuators)
  - New approach to mirror design: start with actuator specification, then design mirror
  - Compatible with existing manufacturing techniques

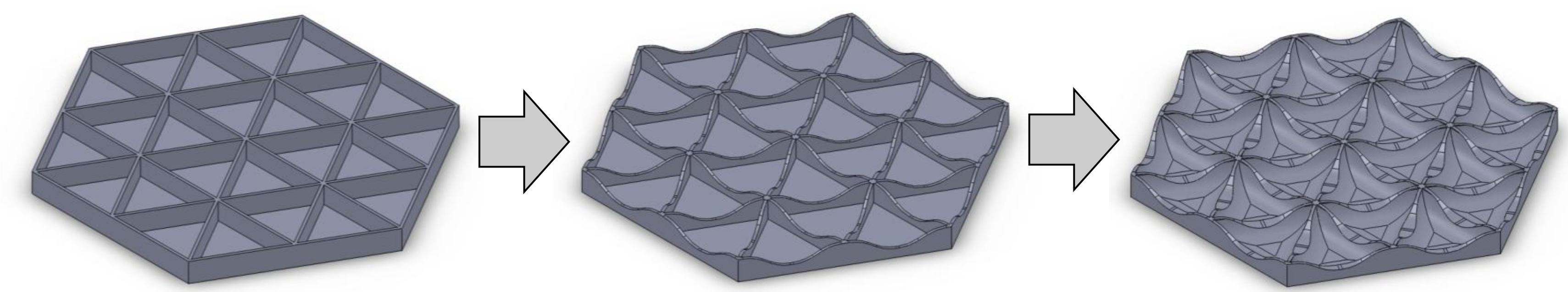

References

[1] National Aeronautics and Space Administration, image archive.

[2] H. Philip Stahl, "JWST Lightweight Mirror TRL-6 Results". *Proc. IEEE Aerospace Conference* (2007).

[3] Mark A. Ealey, "Agile Mandrel Apparatus and Method". US Patent Application No. US 2006/0250672 A1 (2006).

[4] Mark A. Ealey and John A. Wellman, "Highly adaptive integrated meniscus primary mirrors". *Proc. SPIE* 5166 (2004).

[5] Michael J. Shepherd, et al., "Modal Transformation Method for Deformable Membrane Mirrors," *Journal of Guidance, Control, and Dynamics*, Vol. 32, No. 1 (2009).

[6] H. Philip Stahl, "JWST mirror technology development results". *Proc. SPIE* 6671 (2007).

[7] F. Cote, et al., "Dynamic and Static Modelling of Piezoelectric Composite Structures Using a Thermal Analogy with MSC/Nastran", *Composite Structures*, Vol. 65, No. 3 (2004).

[8] Lucy E. Cohan, "Integrated Modeling to Facilitate Control Architecture Design for Lightweight Space Telescopes", *MS Thesis*, MIT (2007).

[9] Lucy E. Cohan, "Integrated Modeling and Design of Lightweight, Active Mirrors for Launch Survival and On-Orbit Performance", *PhD Thesis*, MIT (2010).

[10] Elizabeth Jordan, "Design and Shape Control of Lightweight Mirrors for Dynamic Performance and Athermalization", *MS Thesis*, MIT (2007).

[11] Thomas L. Gray, "Minimizing High Spatial Frequency Residual in Active Space Telescope Mirrors", *MS Thesis*, MIT (2008).

[12] Jason G. Budinoff & Gregory J. Michels, "Design & optimization of the spherical primary optical telescope (SPOT) primary mirror segment", *Proc. SPIE* 5877 (2005).

[13] Bruce H. Dean, et al., "Phase retrieval algorithm for JWST Flight and Testbed Telescope", *Proc. SPIE* 6265 (2006).

[14] Mark A. Ealey and John A. Wellman, "High Authority Deformable Optical System". US Patent Application No. US 2006/0262434 A1 (2006).

[15] Maureen L. Mulvihill and Mark A. Ealey, "Large Mirror Actuators in the 21st Century", *Proc SPIE* 5166 (2004).

[16] Siddarayappa Bikkannavar, et al., "Autonomous phase retrieval control for calibration of the Palomar Adaptive Optics system", *Proc. SPIE* 7015 (2008).

Backup

Model Validation

- Convergence
  - Sensitivity of model outputs to FE mesh density
  - Does the model go to one value as mesh density changes?

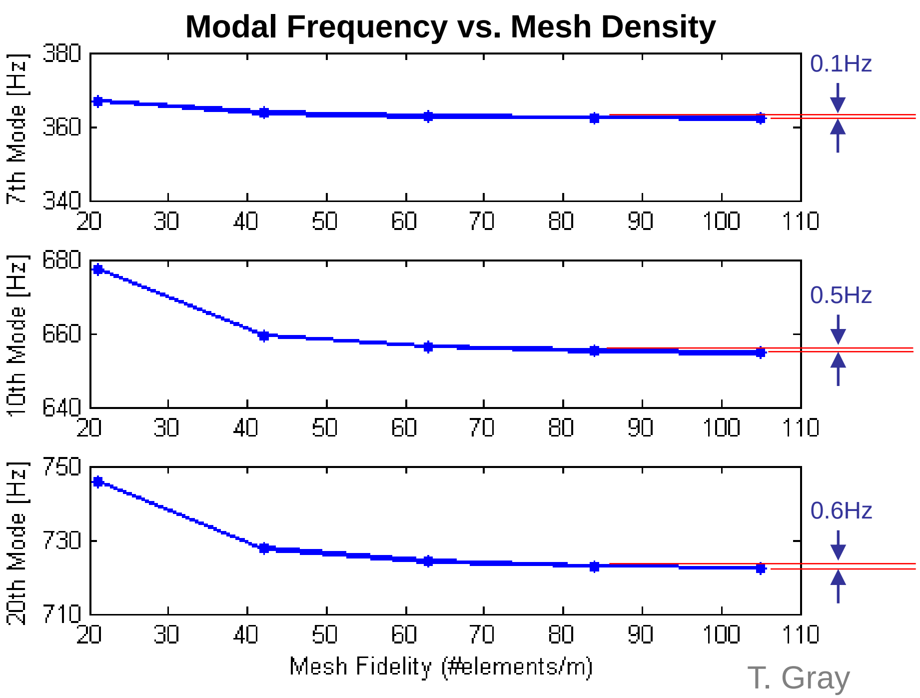

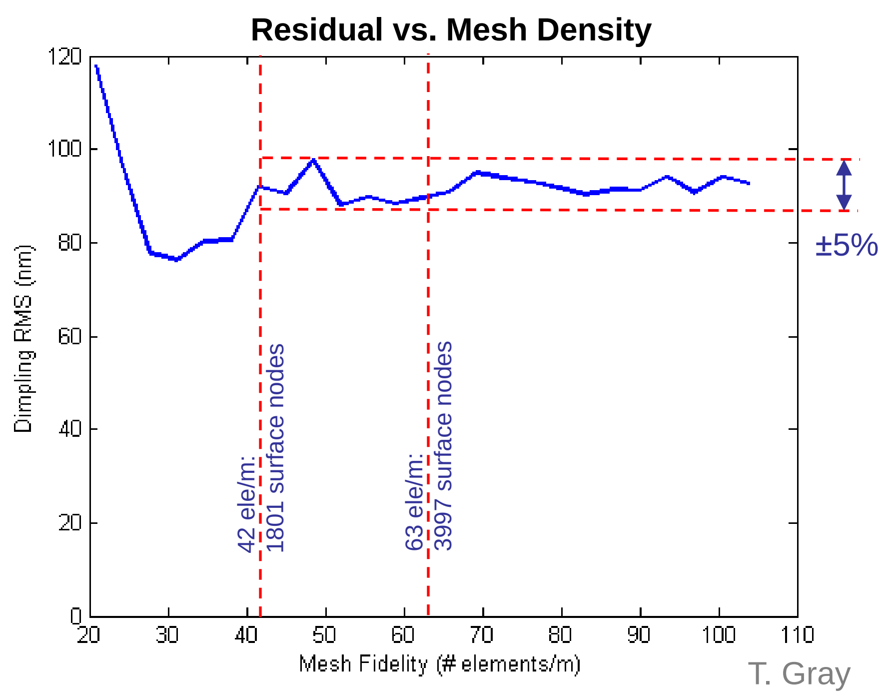

Model Validation (cont.)

- Benchmarking against empirical data
  - Does that one value match real life?

Model output	Error compared to empirical data
Stiffness (fundamental frequency)	2%
Mirror stress due to launch vibration	8%
Residual error for 1 mm ΔROC	7%

Model Validation (cont.)

- Feature-level validation
  - Validate individual features of the model for which there is no “global” test data
  - Compare with first-principles models, published test results, published analysis
  - E.g.: modeling and validation of piezoelectric actuators in [7,9]
  - E.g.: actuator length validation via analytical beam model (below)

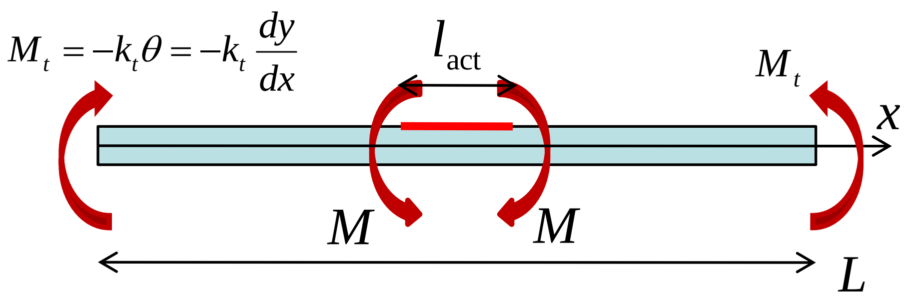

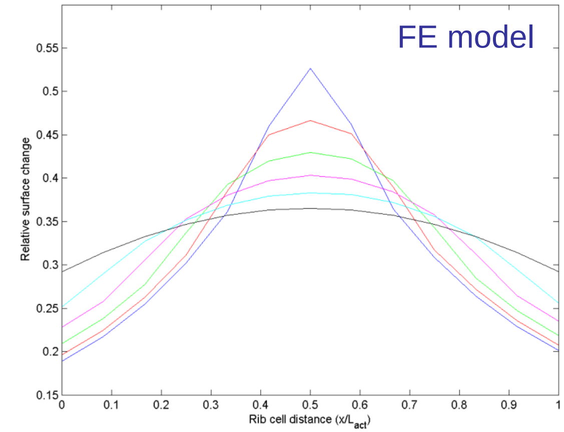

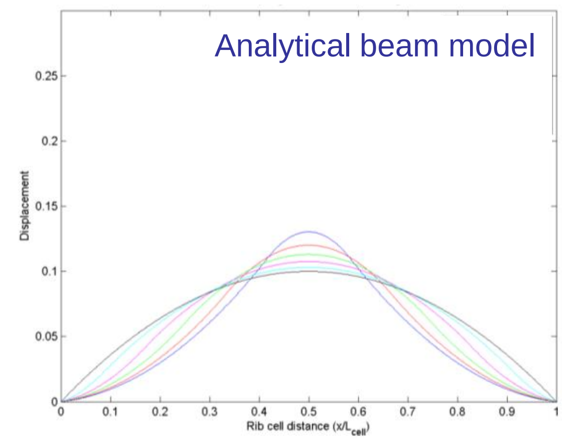

$$y(x) = \frac{M_t}{2EI}x^2 - \frac{M}{2EI}\left\langle x - \frac{L - l_{act}}{2}\right\rangle^2 + \frac{M}{2EI}\left\langle x - \frac{L + l_{act}}{2}\right\rangle^2 + \frac{Ml_{act} - M_t L}{2EI}x$$

$$M_t = \frac{Ml_{act}}{L + EI/k_t}$$

$$\left\langle x - x_0\right\rangle^2 = \begin{cases} 0 & x < x_0 \\ (x - x_0)^2 & x \geq x_0 \end{cases}$$

Baseline Mirror

Parameter	Value
Diameter (flat-flat)	1.0 m
Areal density (SiC only)	8 kg/m^2
Rib rings	4
Primary rib height	25.4 mm
Primary rib thickness	1 mm
Face sheet thickness	1.8 mm
Actuator length	7.2 cm
Actuator length/cell	50%
Number of actuators	156
Radius of curvature	6 m

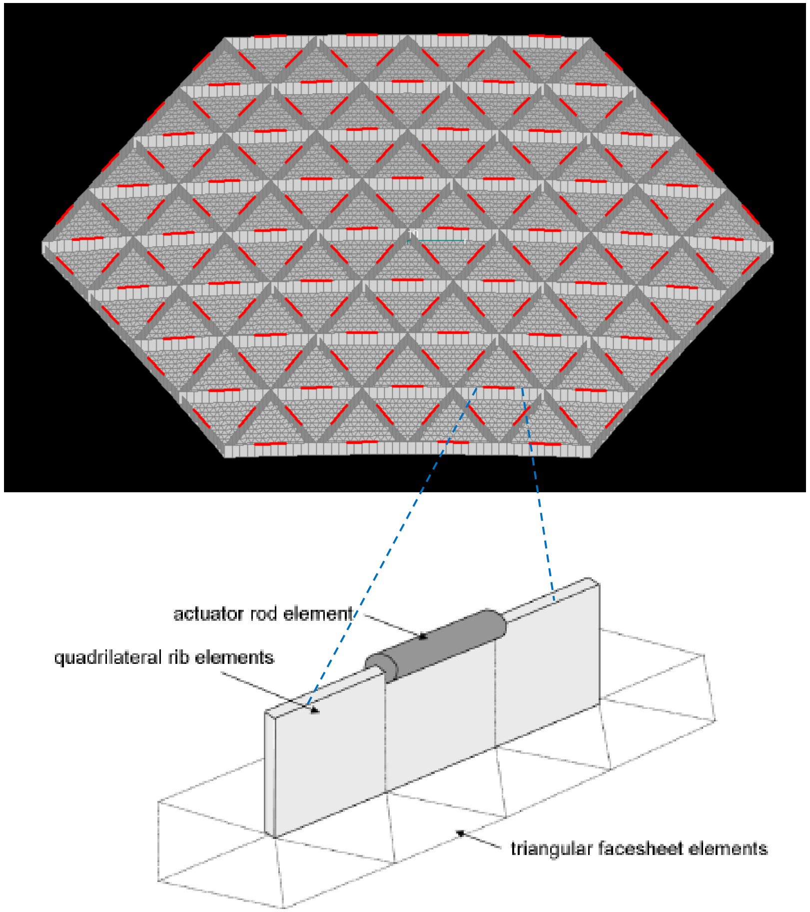

Wavefront Sensing Methods

- Shack-Hartmann Wavefront Sensor
  - Detects the slope of the wavefront by measuring spot displacements
  - Measures the wavefront at discrete locations on the pupil
  - Ignores non-common path errors

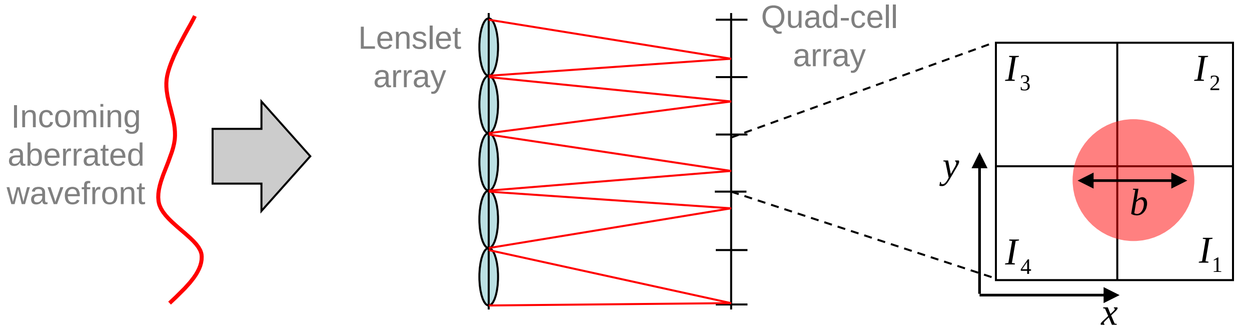

$$\delta_x = \frac{b}{2}\left[\frac{(I_2 + I_1) - (I_3 + I_4)}{I_1 + I_2 + I_3 + I_4}\right]$$

$$\delta_y = \frac{b}{2}\left[\frac{(I_3 + I_2) - (I_4 + I_1)}{I_1 + I_2 + I_3 + I_4}\right]$$

- Modified Gerchberg-Saxton (MGS)
  - Computes wavefront by inverse transforming a defocused point image
  - Uses the focal plane array sampling (more of a continuous map)
  - FT and IFT between image and pupil, enforcing pupil plane image constraints
  - Known defocus removes ambiguity in phase map
  - Captures non-common path errors
  - Baseline method for fine phasing in JWST

- Static Analysis
  - Goal: Compute displacements from known forces and constraints
  - Relate forces to displacements via a global stiffness matrix *K*
  - Build the stiffness matrix from kinematic relationships, Hooke's Law, and force balance

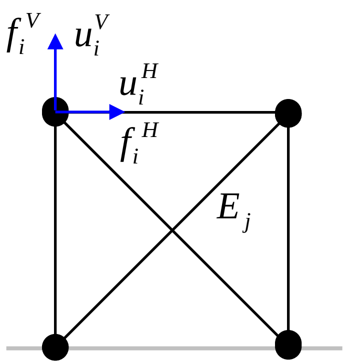

u_i Horizontal and vertical displacements of node *i*

f_i Horizontal and vertical forces acting at node *I*

E_j Elastic modulus of element *j*

Elongations (strain) from displacements

$\boxed{\underline{\varepsilon} = A\underline{u}}$

Internal force (stress) from elongation (strain)

$\boxed{\underline{\sigma} = E\underline{\varepsilon}}$

Force balance (internal and external)

$\boxed{\underline{f} = A^T \underline{\sigma}}$

Force from displacements (combining above equations)

$$\boxed{\begin{aligned} \underline{f} &= A^T E A \underline{u} \\ \underline{f} &= K \underline{u} \end{aligned}} \quad (1)$$

  - Solve (1), typically by elimination

Gilbert Strang, *Computational Science and Engineering*, Wellesley Cambridge Press (2007), pp. 98-104, 187-192.
Mark P. Miller, *MSC/Nastran User's Guide*, 2nd Ed., The MacNeal-Schwendler Corporation (1996), pp. 5-9.

Finite Element Method (cont.)

- Normal Modes Analysis
  - Goal: Compute the normal frequencies and normal modes of a system
  - Transform into an eigenvalue problem

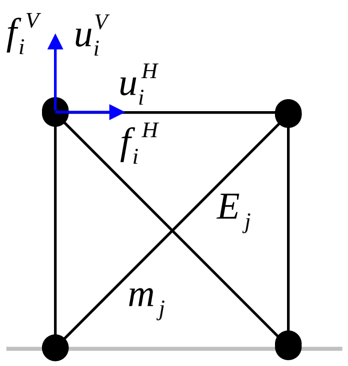

u_i Horizontal and vertical displacements of node *i*

f_i Horizontal and vertical forces acting at node *I*

m_j Mass of element *j*

M Global mass matrix

K Global stiffness matrix (see previous slide)

$$M\underline{\ddot{u}} + K\underline{u} = 0$$

$$\underline{u} = \underline{\phi}\sin\omega t$$

$$\boxed{\left(K - \omega^2 M\right)\underline{\phi} = 0} \quad (2)$$

Last line is an eigenvalue equation of the form $A\underline{x} = \lambda\underline{x}$

  - Solve for normal frequencies (eigenvalues) and normal modes (eigenvectors)

Ken Blakely, *MSC/Nastran Basic Dynamic Analysis*, The MacNeal-Schwendler Corporation (1993), pp. 37-47.

Imaging Consequences

- Impact of residual error on imaging
  - Residual error causes wavefront error (WFE = 2*residual error)
  - This adds an additional phase term to the pupil function
  - Result: degraded image quality via reduced peak energy and image artifacts

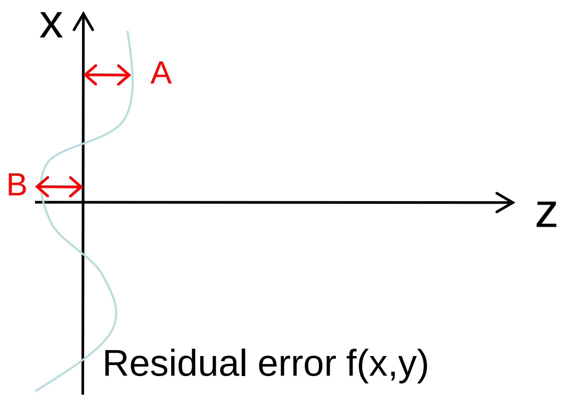

A: Optical "acceleration" → decrease phase

B: Optical delay → increase phase

$$\varphi \text{ [rad]} = -2 * 2\pi/\lambda * f(x,y) \text{ [nm]}$$

No residual

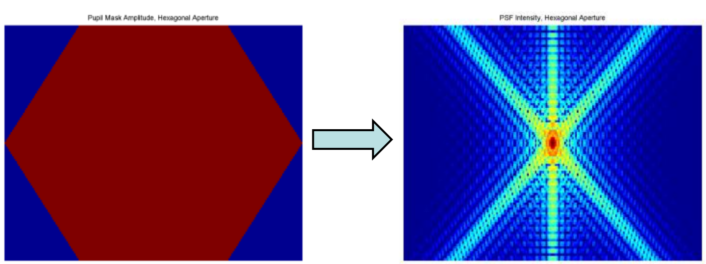

residual for 1mm ΔRoC (baseline)

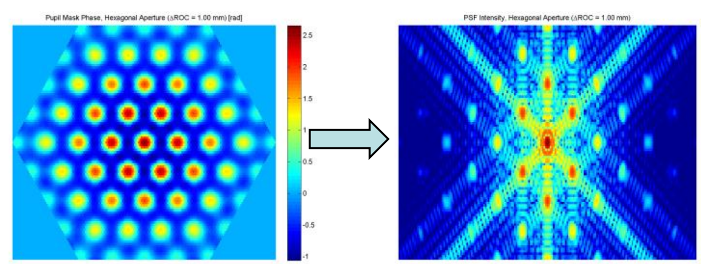

Previous Geometry Results

- Effect of geometric parameters on residual error
  - Number of actuators (rib rings)

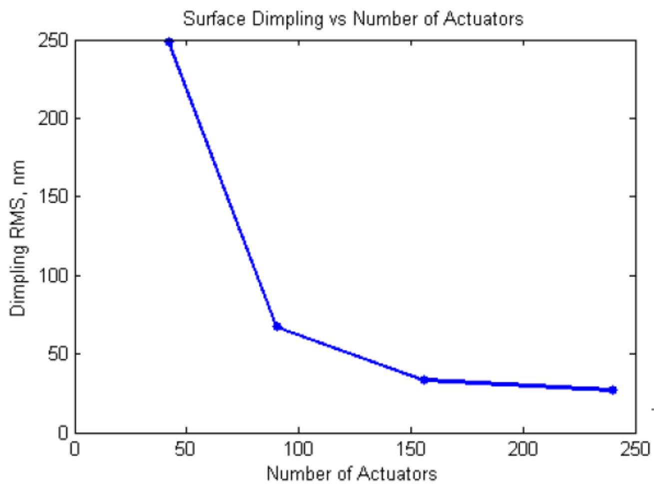

T. Gray

  - Actuator length

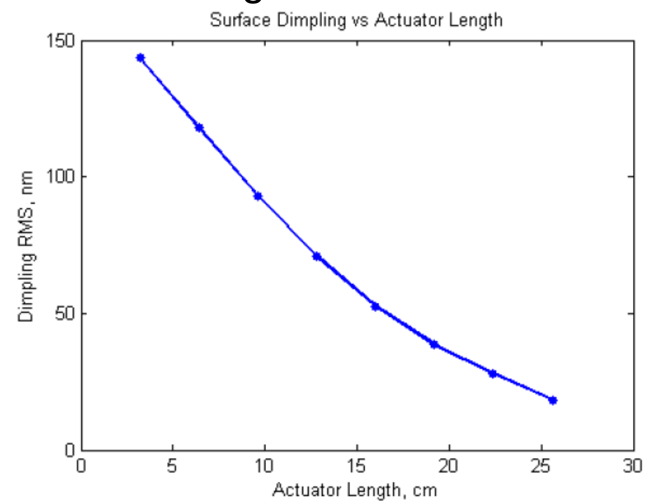

T. Gray

  - Areal density

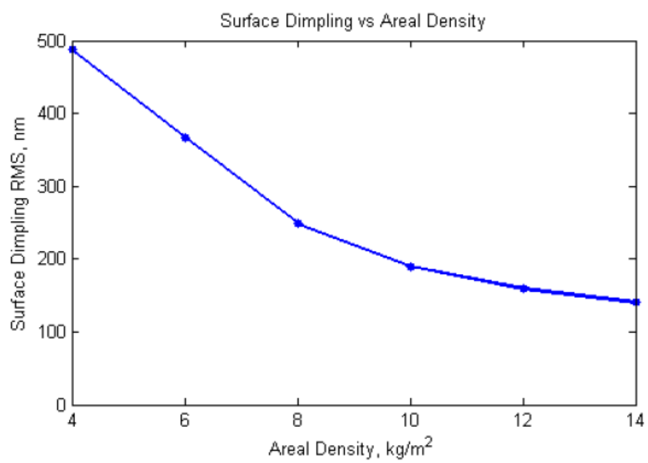

T. Gray

  - Rib height

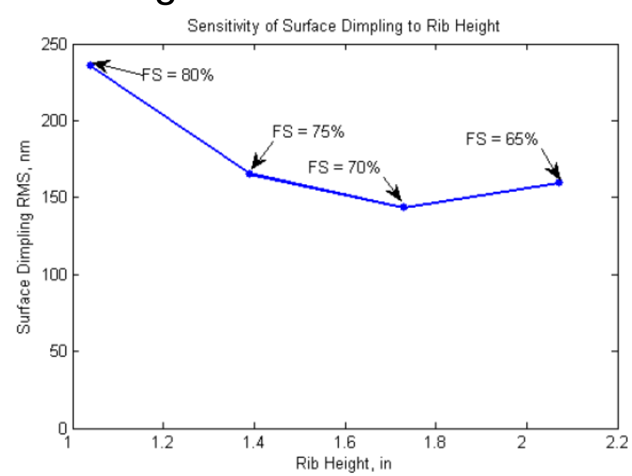

T. Gray

Actuator Length

- Changing actuator length
  - Longer actuators give better performance
  - Increasing actuator length increases the distance between the applied moments, smoothing the commanded shape

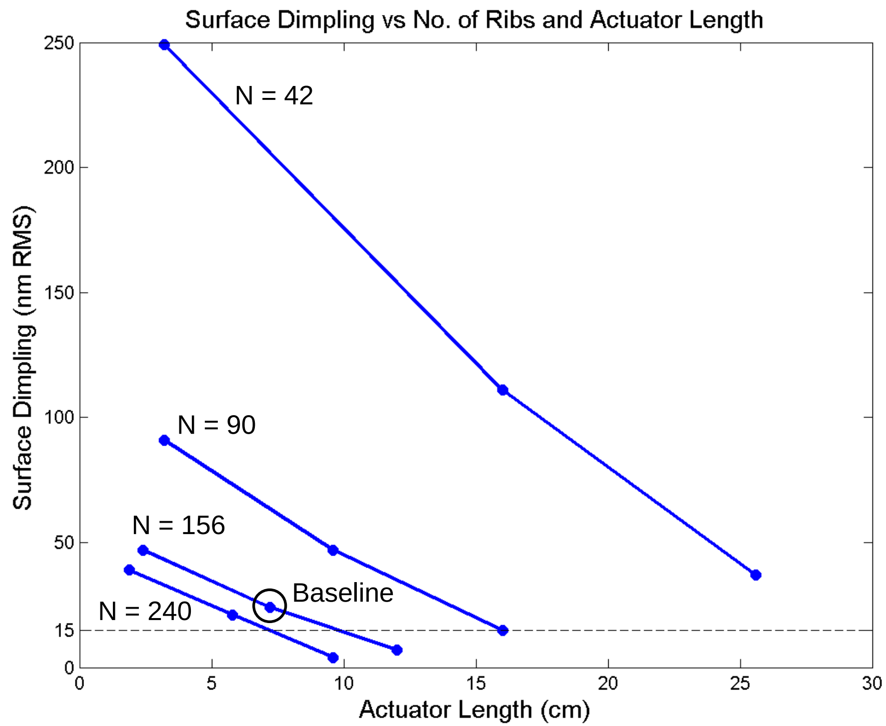

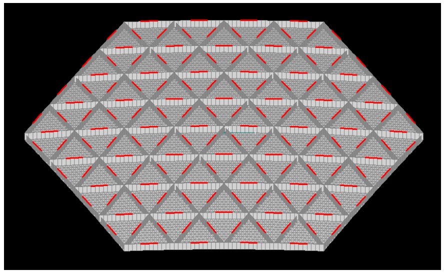

Rib “rings”	Actuators
2	42
3	90
4	156
5	240

Actuator Length (cont.)

- Changing actuator length
  - Longer actuators give better performance (3.6x improvement over the baseline)
  - Increasing actuator length increases the distance between the applied moments, smoothing the commanded shape

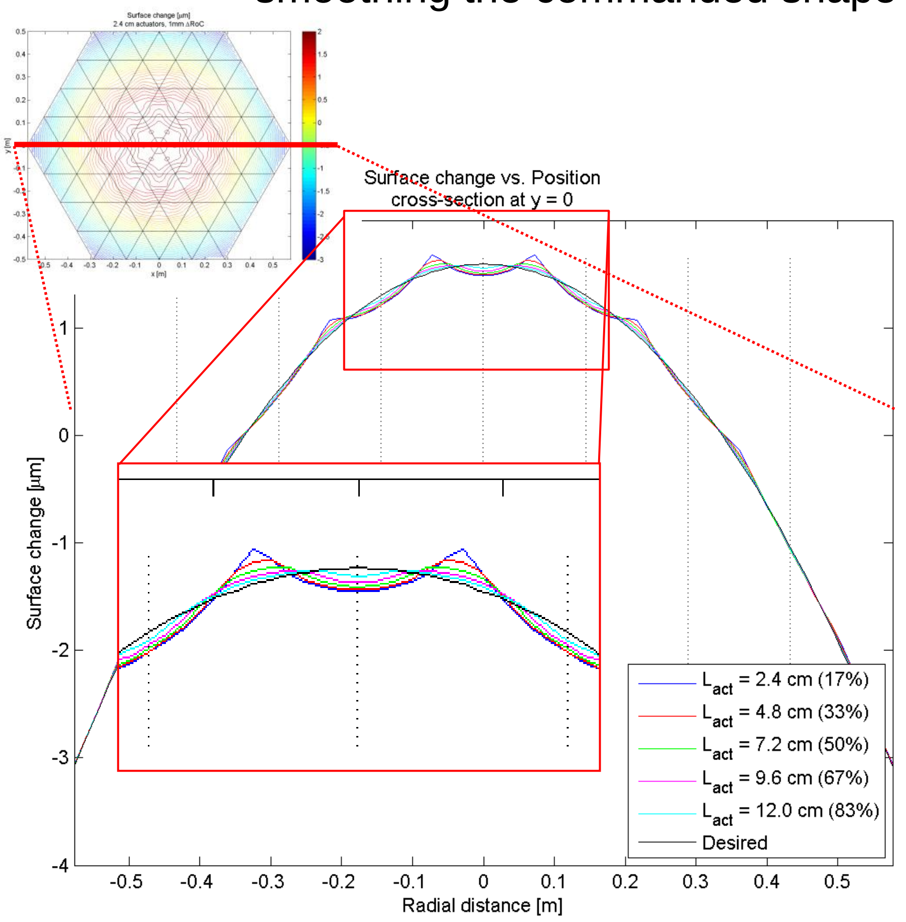

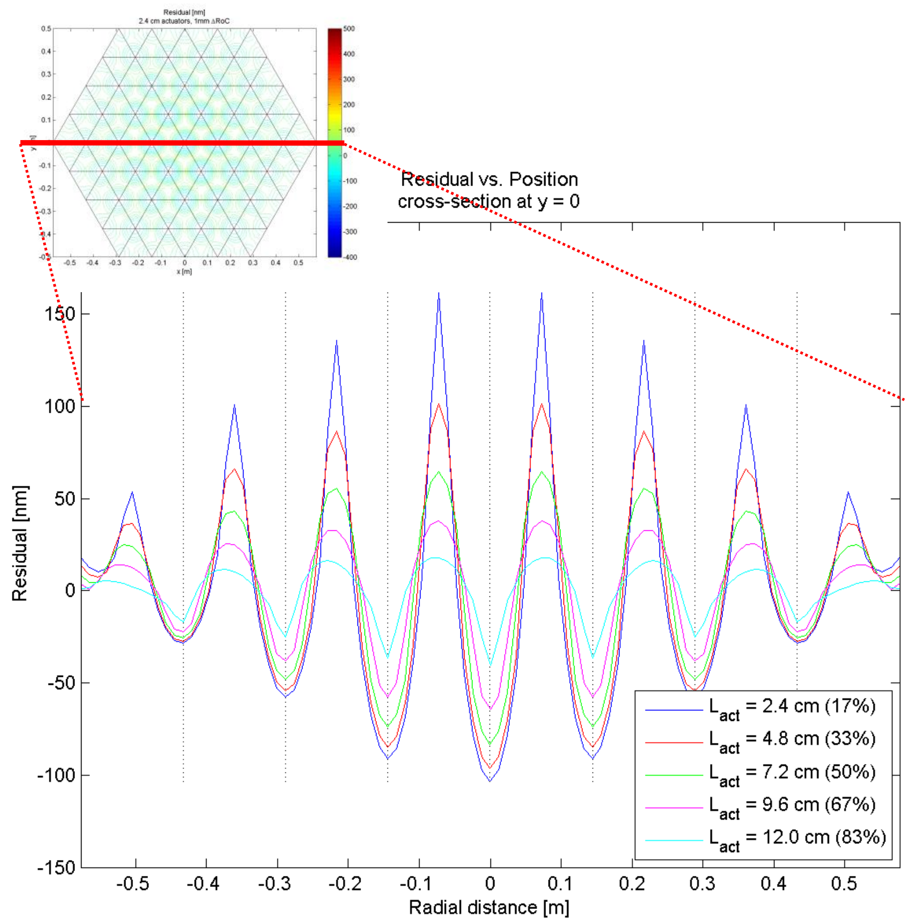

 26 January 2010

Actuator Length (cont.)

- Beam model
  - Single rib cell modeled; actuator modeled as a moment couple
  - As space between couple increases, more of the beam experiences parabolic deflection
  - Influence function becomes less localized

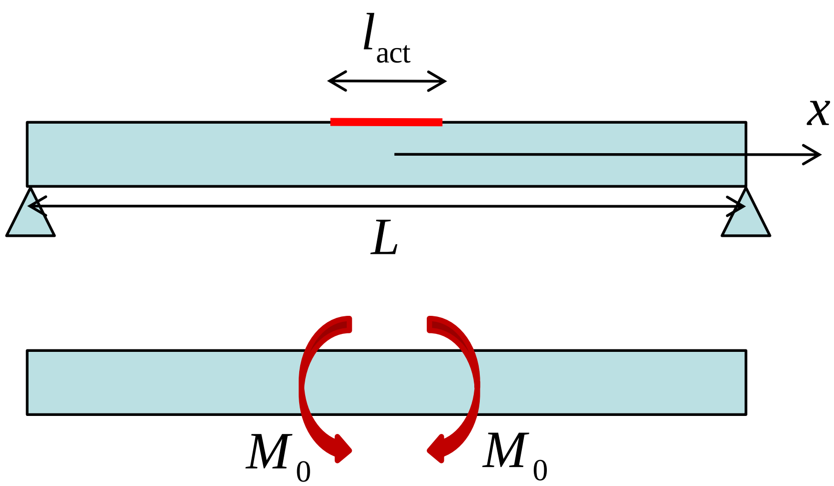

$$y(x)=\frac{M_0}{2EI}\left\langle x-\frac{a+l_{act}}{2}\right\rangle^2-\frac{M_0}{2EI}\left\langle x-\frac{a-l_{act}}{2}\right\rangle^2+\frac{M_0 l_{act}}{EI}\left(1-\frac{a}{2L}\right)x$$

$$\langle x-x_0\rangle^2=\begin{cases}0 & x<x_0\\ (x-x_0)^2 & x\ge x_0\end{cases}$$

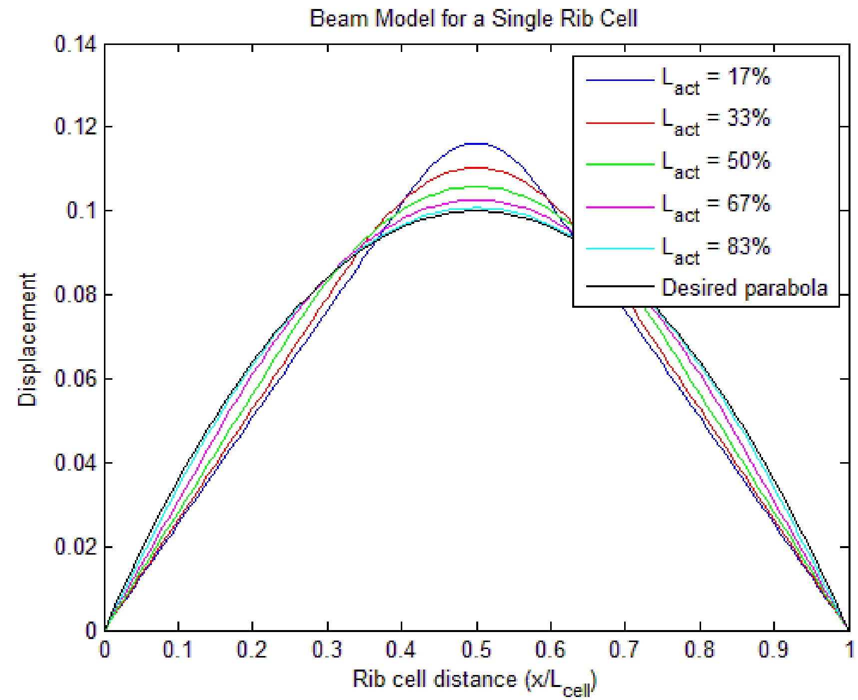

Initial Blending Results

- Rib-to-facesheet blending
  - Idea: smooth the transition from rib to facesheet spread the influence of a given actuatc
  - Initial implementation: Use 2D shell elements but vary the thickness to approximate 3D blending
- Implementation details:

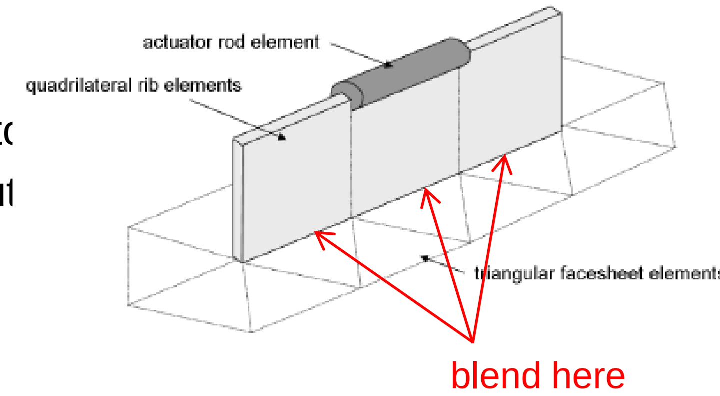

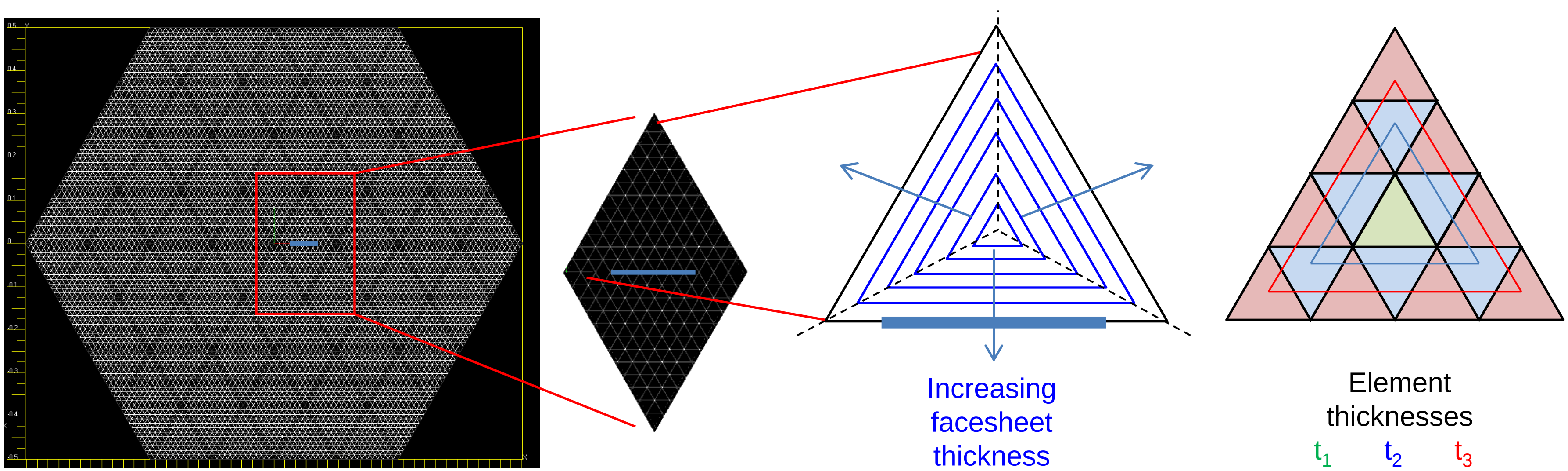

Initial Blending Results (cont.)

- Rib-to-facesheet blending
  - Idea: smooth the transition from rib to facesheet spread the influence of a given actuator
  - Initial implementation: Use 2D shell elements but vary the thickness to approximate 3D blending
- Results:
  - Increases the “vertical” extent of the actuator’s influence function

No blending With blending

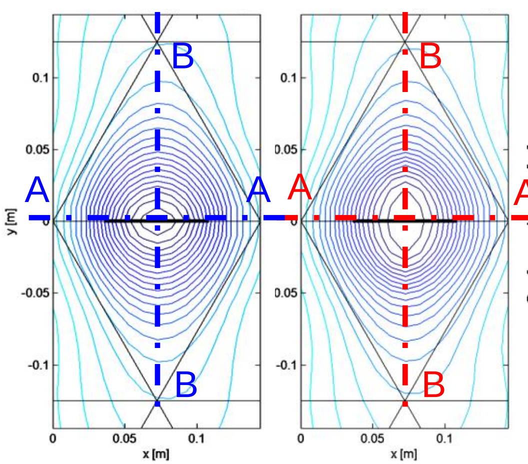

Slice A-A (horizontal)

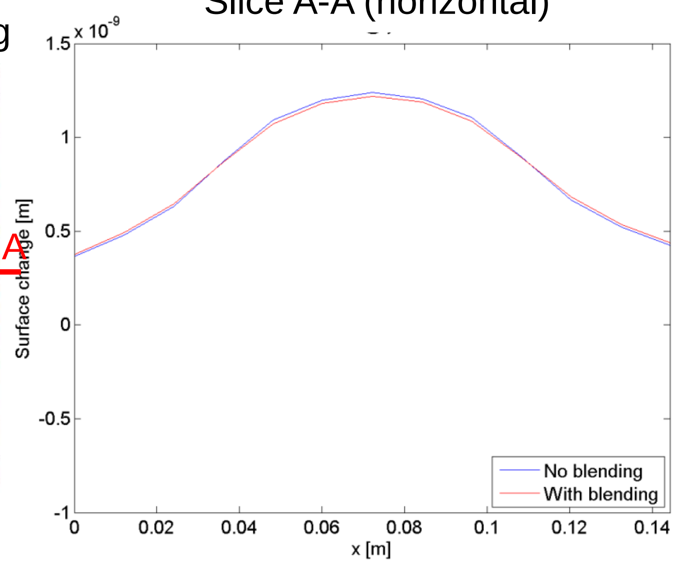

Slice B-B (vertical)

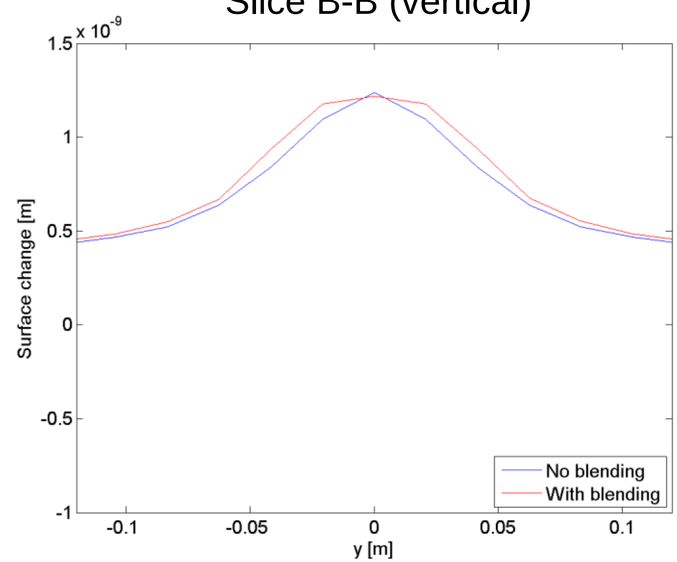

Patch Actuator

- 2D patch actuator
  - Idea: use a thin piezoelectric patch and take advantage of the d_{31} behavior
  - Place within the cells to add another set of influence functions
  - Initial implementation: Use 2D shell elements attached at nodes

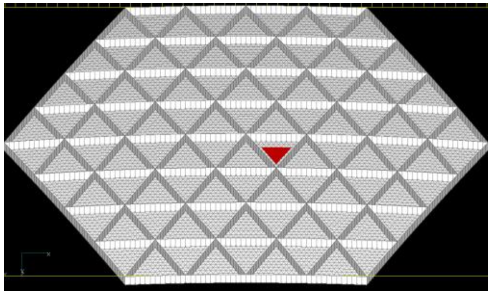

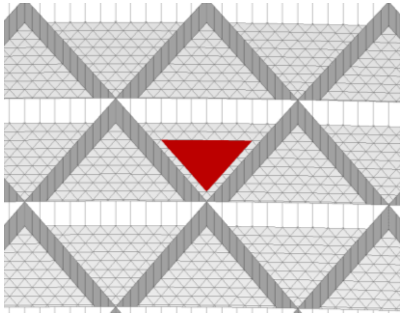

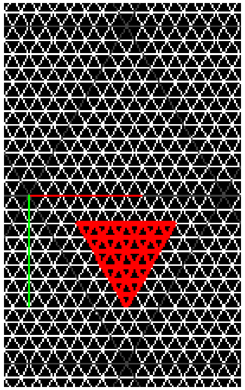

- Results
  - Well-defined influence function within the rib cell

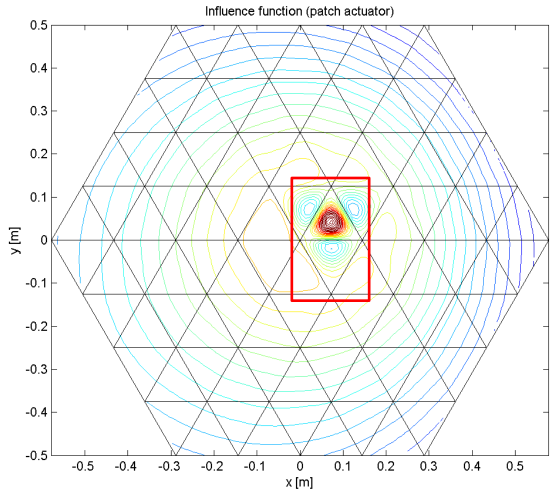

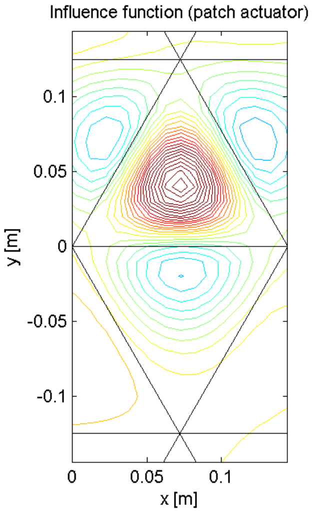

SPOT

- <u>S</u>pherical <u>P</u>rimary <u>O</u>ptical <u>T</u>elescope
  - NASA Goddard
  - Single segment test bed

Non-optimized mirror shape

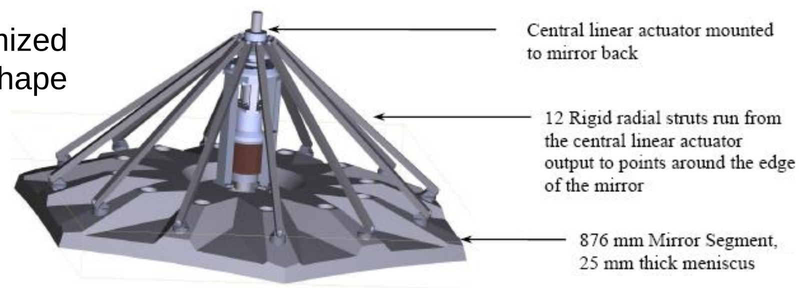

Figure shape	sphere
Diameter	0.876 m
RoC	5 m (nominal)
Max surface error for 400 µm ΔRoC	15 nm RMS
Material	Pyrex
Minimum areal density (10 mm thickness throughout)	22.3 kg/m^2 (Pyrex only)

Residual in non-optimized mirror

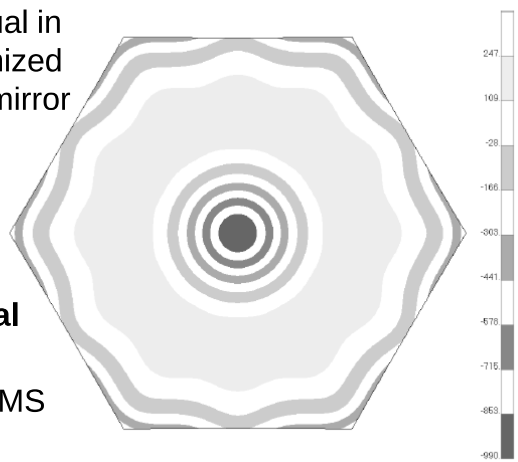

Residual error:
225 nm RMS

Select basis functions

$f(r) = a_1 r + a_2 r^2 + a_3 r^3 + \ldots$

$g(\theta) = b_1 \sin(6\theta) + b_2 \sin(12\theta)$

Optimize to find coefficients

Optimized shape

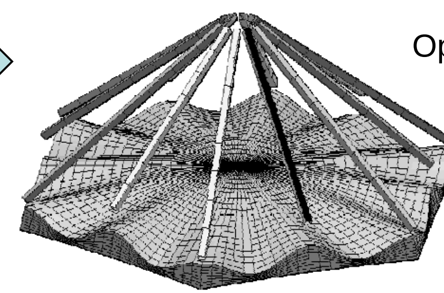

Residual error:
30.6 nm RMS

Jason G. Budinoff, Gregory J. Michels, "Design & Optimization of the Spherical Primary Optical Telescope (SPOT) Primary Mirror Segment", *Proc. SPIE,* Vol. 5877 (2005).

Trade Space Exploration

- Past MOST results
  - Parametric space telescope model
    - Primary mirror and kinematic mounts
    - Secondary mirror and support tower
    - Solar arrays and bus
  - Allows rapid tradespace exploration
  - Compare designs and identify driving parameters

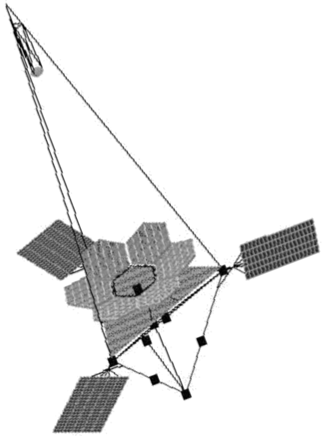

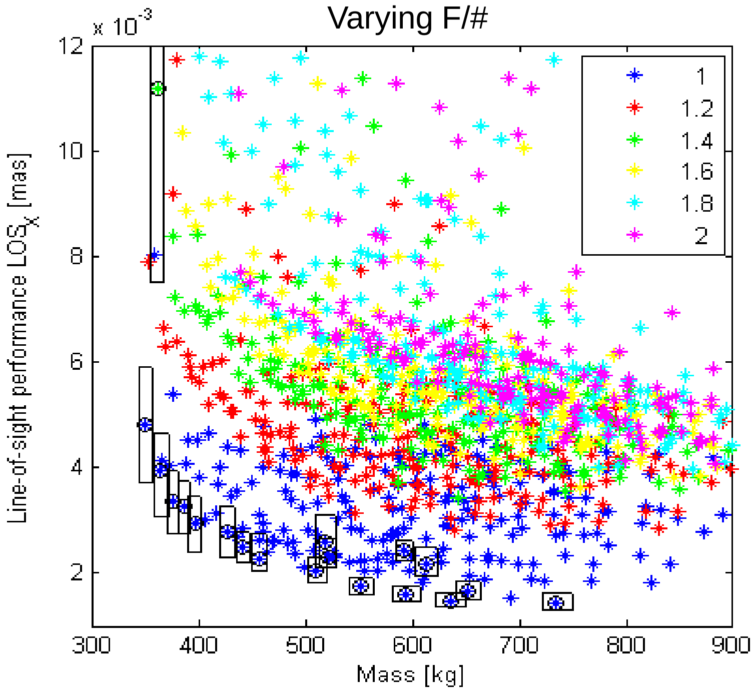

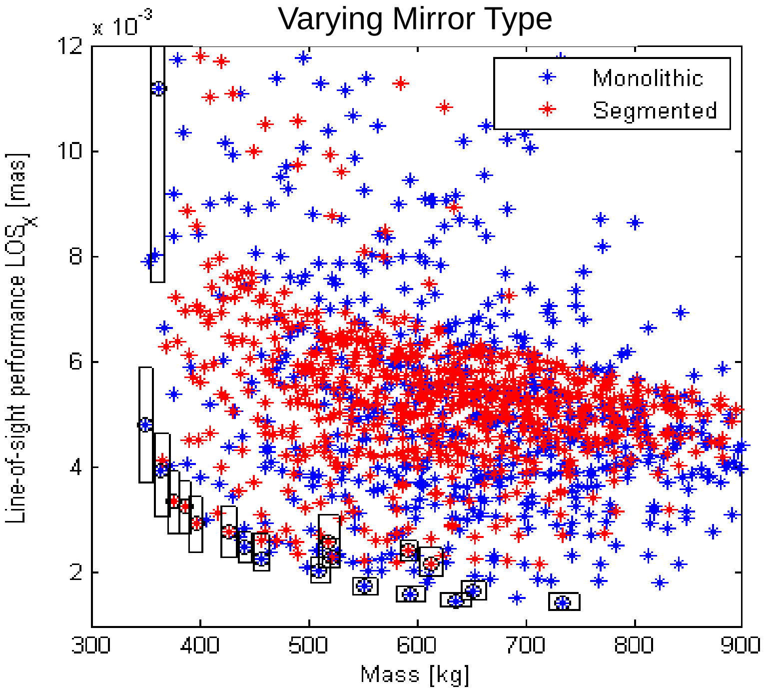

Scott A. Uebelhart, "Non-Deterministic Design and Analysis of Parameterized Optical Structures during Conceptual Design", *PhD Thesis,* MIT (2006)